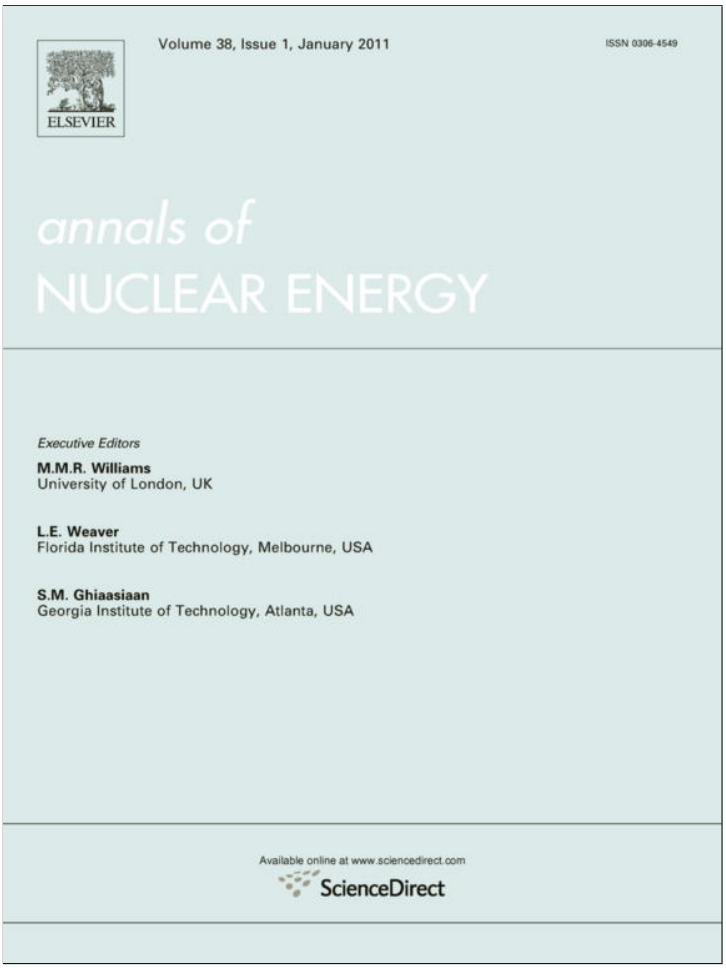

(This is a sample cover image for this issue. The actual cover is not yet available at this time.)

Annals of Nuclear Energy 39 (2012) 70–82

Contents lists available at SciVerse ScienceDirect

Annals of Nuclear Energy

journal homepage: www.elsevier.com/locate/anucene

Application of a new drag coefficient model at CFD-simulations on free surface flows relevant for the nuclear reactor safety analysis

Deendarlianto [a,b,*], Thomas Höhne [a], Pavel Apanasevich [a], Dirk Lucas [a], Christophe Vallée [a], Matthias Beyer [a]

[a] Helmholtz-Zentrum Dresden-Rossendorf e.V., Institute of Safety Research, P.O. Box 510 119, D-01314 Dresden, Germany
[b] Department of Mechanical & Industrial Engineering, Faculty of Engineering, Gadjah Mada University, Jalan Grafika No. 2, Yogyakarta 55281, Indonesia

ARTICLE INFO

Article history:
Received 27 April 2011
Received in revised form 12 September 2011
Accepted 12 September 2011

Keywords:
Computational fluid dynamics (CFD)
Algebraic interfacial area density (AIAD) model
Drag coefficient
Pressurized water reactor (PWR)
Hot leg
Cold leg

ABSTRACT

This paper presents different CFD-simulations on flows which are relevant for nuclear reactor safety using a new modeling approach for the interfacial drag at free surfaces. The developed drag coefficient model was implemented together with the Algebraic Interfacial Area Density (AIAD) model (Höhne, 2009) into the three-dimensional (3-D) computational fluid dynamics (CFD) code ANSYS-CFX. The applications considered include the prediction of counter-current flow limitations (CCFL) in a PWR hot leg, the development of hydraulic jump during the air–water co-current flow in a horizontal channel, and pressurized thermal shock (PTS) phenomena in a PWR cold leg and downcomer. For the modeling of these tasks, an Euler–Euler approach was used. This approach allows the use of different models depending on the local morphology. In the frame of an Euler–Euler simulation, the local morphology of the phases has to be considered in the drag model.

To demonstrate the feasibility of the present approach, the computed main parameters of each case were compared with experimental data. It is shown that the CFD calculations agree well with the experimental data. This indicates that the AIAD model combined with new drag force modeling is a promising way to simulate the phenomena in frame of the Euler–Euler approach. Moreover the further validation of the model by including mass transfer effects should be carried out.

1. Introduction

The importance of numerical simulations different technical systems was clearly increased during the last two decades. In this context, the use of computational fluid dynamics (CFD) codes to predict horizontal two phase flows in nuclear reactors such as slugging, counter-current flow limitations (CCFL), and pressurized thermal shocks (PTS) related phenomena tends to be of increasing interest. The detailed three-dimensional (3-D) information on the particular phenomena becomes a new requirement in the reactor safety analysis. CFD allows substituting geometry-dependent empirical closure relations with more physically justified closure laws that are formulated at the scale of the structures of the gas–liquid interface. In this way, CFD is more flexible than one-dimensional analytical solution, in terms of transferability of models to changes in geometrical and thermodynamic boundary conditions. Meanwhile the implementation of the CFD tools becomes a critical issue if we are interested in the physically meaning of the local problems.

Various multidimensional numerical models were developed to simulate stratified flows: Marker and Cell (Harlow and Welch, 1965), Volume of Fluid method (VOF) (Hirt and Nichols, 1981) and Level set method (Osher and Sethian, 1988). These methods can in principle capture accurately most of the physics of the stratified flows. One of the first attempts to simulate mixed flows was presented by Cerne et al. (2001) who coupled the VOF method with a two-fluid model in order to bring together the advantages of the both analytical formulations. Štrubelj et al. (2009) reported about simulations of free surface flows with implementation of surface tension and interface sharpening in the two-fluid model. Coste et al. (2010) introduced a Large Interface Method into the two phase flow CFD code NEPTUNE_CFD.

A subset of the present authors (Deendarlianto et al., submitted for publication) has already reviewed different applications of CFD codes to simulate the phenomena around the counter-current flow limitations (CCFL) in a pressurized water reactor (PWR) hot leg. They indicated that there is still a lack of knowledge regarding suitable closure models for this application. For this reason in some cases also empirical correlations originally obtained for one-dimensional codes are used for the multidimensional problem.

* Corresponding author at: Helmholtz-Zentrum Dresden-Rossendorf e.V., Institute of Safety Research, P.O. Box 510 119, D-01314 Dresden, Germany. Tel.: +49 351 260 3291; fax: +49 351 260 13291.
E-mail address: deendarlianto@ugm.ac.id (Deendarlianto).

0306-4549/$ - see front matter © 2011 Elsevier Ltd. All rights reserved.
doi:10.1016/j.anucene.2011.09.010

The development of a general model closer to physics and including less empiricism is a long-term objective of the activities of the *Helmholtz-Zentrum Dresden-Rossendorf* (*HZDR*) research programs. Such models are an essential precondition for the application of CFD codes to the modeling of flow related phenomena in nuclear facilities. Here local geometry independent models for mass, momentum, heat transfer, and scalar transport are developed and validated. The new formulation for the drag force at the free surface within the algebraic interfacial area density model (AIAD) developed by Höhne (2009) is one result of these activities.

The paper presents some examples for the application of the new drag coefficient in frame of the AIAD model for issues relevant for nuclear reactor thermal hydraulics. The simulations were carried out using ANSYS CFX the frame of a scientific partnership between *HZDR* and *ANSYS Germany*. Based on this partnership the models developed are implemented into the code and thus contribute to the code qualification. The following topical issues, will be briefly discussed in the paper:

1. Gas–liquid counter-current two-phase flow in a PWR hot leg channel.
2. Hydraulic jump development during the air/water co-current flow in a horizontal channel.
3. Pressurized thermal shock phenomena in a PWR cold leg and downcomer.

In the present paper, the philosophy of free surface modeling in inhomogeneous two-phase flow model will be introduced firstly. Next, the derivation of new drag coefficient in AIAD model framework will be presented. Finally, the validation result and future work on this context will be discussed.

2. Computational modeling

In the present test cases, the flow is treated as transient according to the experimental conditions. The problem is a three dimensional (3-D) that has to be solved by applying multiphase CFD methods. Such multiphase methods resolve the conservation equations for mass, momentum and energy and they are distinguished by the different approaches and strategies used in describing the physical closure models. For the solution of the described task, Euler–Euler approach was used. This approach assumes that at least two fluids are continuously penetrating each other. The volume fraction of the fluids in each cell sums to unity. For each fluid, the full set of conservation equations is solved. Therefore, each fluid has a different velocity field. The mechanisms of the interaction of the fluids are the momentum transfer modeled by the flow resistance, the mass transfer modeled by phase change and the energy transfer modeled by heat conduction. In the present works the both phases are assumed adiabatic and incompressible; therefore, the two latter interactions in the present problem are not relevant.

In the calculation, we solved the conservation and momentum equations of the two-fluid model, which have the following form

$$\frac{\partial \alpha_k \rho_k}{\partial t} + \nabla \bullet (\alpha_k \rho_k U_k) = 0 \tag{1}$$

$$\frac{\partial \alpha_k \rho_k}{\partial t} + \nabla \bullet (\alpha_k \rho_k U_k U_k) = -\alpha_k \nabla p_k + \alpha_k \rho_k g + \nabla \alpha_k (\tau^v + \tau_k^t) - \nabla \alpha_k \cdot \tau_{D_k} \tag{2}$$

where the subscript k denotes phase gas or liquid, ρ is the density, u is the velocity vector, t is the time, p is the pressure, g is the gravitational acceleration, α is the volume fraction, τ is the shear stress (τ^v is the average viscous shear stress, τ^t is the turbulent shear stress) and τ_D is the interfacial shear stress.

In simulation of separated two-phase flow, the gas bubble in the liquid can be resulted by the drag force. The total drag force is derived from the interfacial shear stress ($F_D = \tau_D \cdot A$), is most conveniently expressed in terms of the dimensionless drag coefficient C_D

$$F_D = \frac{1}{2} C_D A \rho_{LG} |(U_L - U_G)|^2 \tag{3}$$

where ρ_{LG} is the average density, $|(U_L - U_G)|$ is the relative velocity and A is the projected area of the body in flow direction.

3. Free surface & AIAD model

Höhne and Vallée (2010) noted that the CFD simulation of the free surface can be performed by using the multi-fluid Euler–Euler modeling approach available in *ANSYS CFX*. However it requires a careful treatment of several aspects of the model. Those are interfacial area density, turbulence model near free surface and interphase momentum models. The separate models are also necessary for dispersed particles and separated continuous phases (interfacial drag, etc.). The suitable methodology within the Euler–Euler approach is to use the momentum exchange coefficient depends on the local morphology. Here Egorov (2004) proposed an Algebraic Interfacial Area Density (AIAD) model to solve the above problem. The conceptions of the proposed model are:

- The interfacial area density allows the detection of the morphological form and the corresponding switching for each correlation from one object pair to another.
- It provides a law for interfacial area density and the drag coefficient for full range of phase volume fraction of gas or liquid ($0 \leqslant \alpha_G \leqslant 1$) as shown in Fig. 1. Here the interfacial area density in the intermediate range is also set to the interfacial area density for the free surface.
- The model improves the physical modeling in the asymptotic limits of bubbly and droplet flows.

The interfacial area density A also depends on the morphology of the phases. For bubbles, the interfacial area density is defined as follows:

$$A_B = \frac{6\alpha_G}{d_B} \tag{4}$$

Here d_B is the bubble diameter and α_G is the gas void fraction.

For a free surface an important requirement for the model is the normalizing condition: the volume integral of the area density must be equal to the real surface area. It means that integration of the area density along a normal to the surface must yield unity ($\int_{-\infty}^{+\infty} A dn = 1$). Next, the interfacial area density is defined as absolute value of the gradients of the liquid fraction in x, y and z directions, and is written as,

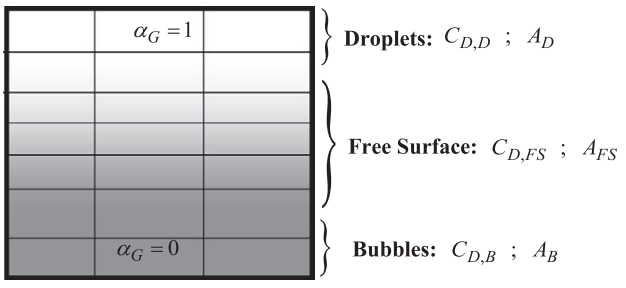

Fig. 1. Morphologies in AIAD model.

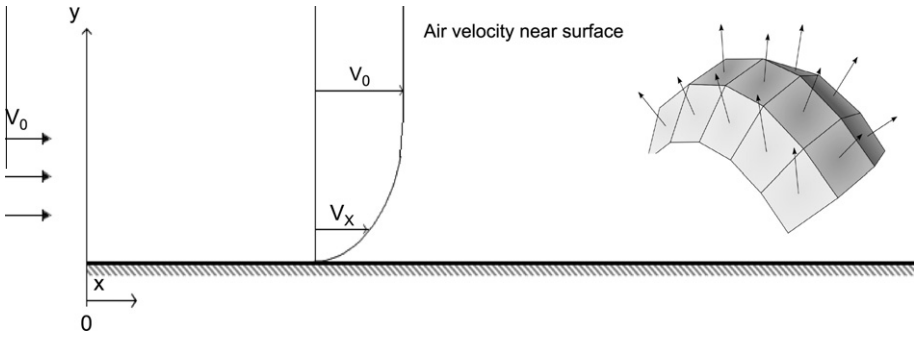

Fig. 2. Air velocity near the free surface (Höhne and Vallée, 2010).

$$A_{FS} = |\nabla \alpha_L| = \sqrt{\left(\frac{\partial \alpha_L}{\partial x}\right)^2 + \left(\frac{\partial \alpha_L}{\partial y}\right)^2 + \left(\frac{\partial \alpha_L}{\partial z}\right)^2} \tag{5}$$

Next, the average density ρ_{LG} is defined as

$$\rho_{LG} = \rho_G \alpha_G + \rho_L (1 - \alpha_G) \tag{6}$$

where ρ_L and ρ_G are the liquid and gas densities, respectively. In the bubble regime, where the α_G is low, the average density according to Eq. (6) is close to liquid phase density ρ_L. According to the flow regime (bubbly flow, droplet flow or stratified flow with a free surface), the corresponding drag coefficients and area densities have to be applied.

The simples switching procedure for the interfacial area density uses the blending function f. Such functions introduce void fraction limits, the weight for flow regimes and length scales for bubbly and droplet flow, which are defined as:

$$f_B = \frac{1}{1 + e^{A_B(\alpha_G - \alpha_{B,\text{limit}})}} \tag{7}$$

$$f_D = \frac{1}{1 + e^{A_D(\alpha_G - \alpha_{D,\text{limit}})}} \tag{8}$$

The blending function for the free surface is defined as

$$f_{FS} = 1 - f_B - f_D \tag{9}$$

The area density and the drag coefficient are respectively well defined in the domain by

$$A = f_{FS} A_{FS} + f_B A_B + f_D A_D \tag{10}$$

$$C_D = f_{FS} C_{D,FS} + f_B C_{D,B} + f_D C_{D,D} \tag{11}$$

In simulation of free surface flows, Eq. (3) does not represent a realistic physical model. It is reasonable to expect that the velocities of both fluids in the vicinity of the interface are rather similar. To achieve this result, it is assumed that the shear stress near the surface behaves like a wall shear stress on both sides of the interface in order to reduce the velocity differences of both phases.

Höhne (Höhne and Vallée, 2010) derived a new drag coefficient in the AIAD model for the free surface application. In his proposal, a shear stress like a wall shear stress is assumed near the surface from both sides to reduce the velocity differences of both phases as shown in Fig. 2. Here, a viscous fluid moving along a "solid" like boundary will incur a shear stress, the no-slip condition, the morphology region "free surface" is the boundary layer, the shear stress is imparted onto the boundary as a result of this loss of velocity.

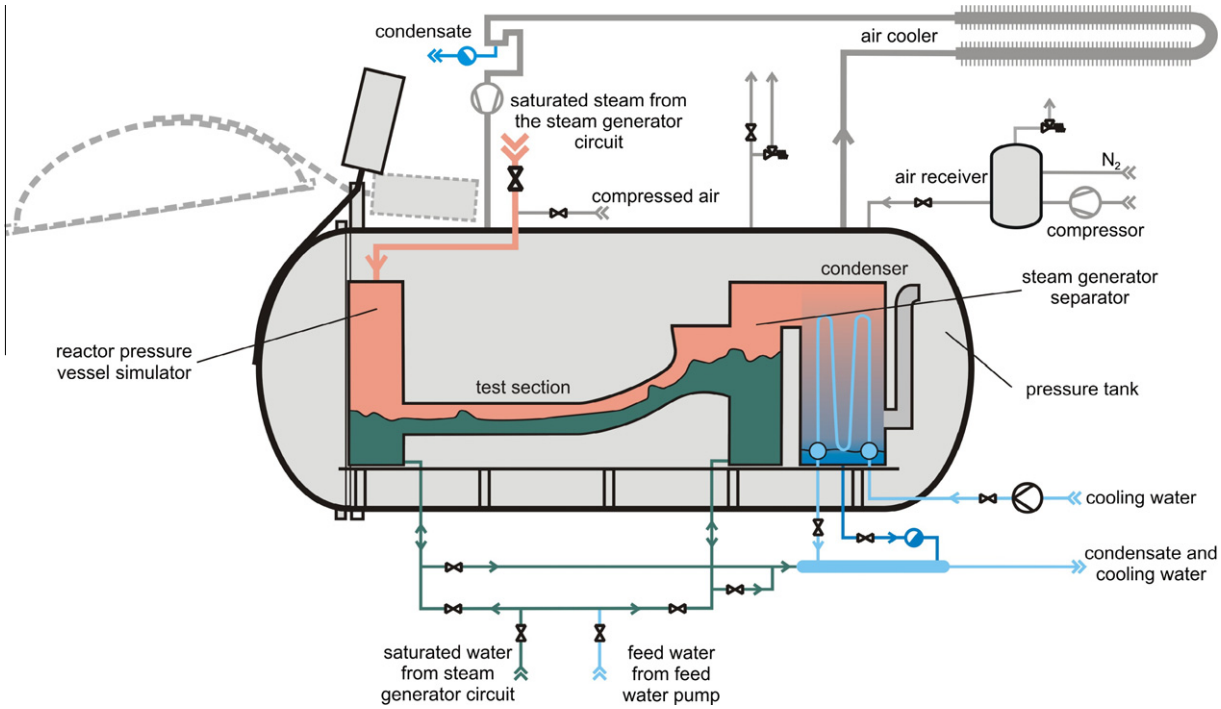

Fig. 3. Schematic diagram of CCFL experiment (Deendarlianto et al., 2008).

$$\tau_{W,k} = \mu_k \left.\frac{\partial u_k}{\partial y}\right|_{y=0} \quad (12)$$

where y points are in the normal directions of the free surface. Finally, the drag coefficient of the free surface can be obtained from the substitution of the Eqs. (3), (5), and (12) and is locally dependent on the fraction of phases, liquid density, and the slip velocity between the phases.

$$C_{D,FS} = \frac{2(\alpha_L \tau_L + \alpha_G \tau_G)}{\rho_{LG} U_{slip}^2} \quad (13)$$

where wall shear stresses of the gas and liquid τ_L and τ_G onto the free surface are a function of the viscosity of both phases, the area of free surface and the gradient of void fraction in x, y, and z axes. In the simulation, the drag coefficient of the bubble, a constant value of $C_{D,B} = 0.44$ was taken, based on the drag of rigid spheres at the medium to high Reynolds number regime. For the drag coefficient of the droplet, the $C_{D,D} = 0.44$ is also taken. On the other hand, the drag coefficient of the free surface, $C_{D,FS}$, refers to Eq. (13).

4. CFD simulations and discussion

4.1. Gas–liquid counter-current two-phase flow in a PWR hot leg

Numerical investigation on gas–liquid counter-current two-phase flow in a PWR hot leg has been performed during last two decades. Those were performed in commercial CFD codes by solving two-fluid model of in 2-D (Wang and Mayinger, 1995) and 3-D (Minami et al., 2009; Murase et al., 2009). In their simulations, the interfacial friction factors were adopted from the empirical correlations obtained from literatures on the basis of 1-D analysis, which might has some limitations on the interfacial transfer and the descriptions of local physic. In the present work, we have simulated the similar phenomena for a flat model of hot leg which represents the geometry of a 1:3 scale Konvoi reactor (Fig. 3). In general, the results have been described in previous study (Deendarlianto et al., in press), and main features will be presented in the present paper.

For the experimental investigation, a hot leg channel with rectangular cross section was built at transient TwO Phase FLOW

Table 1
Calculation runs.

HZDR exp. run	m_L (kg/s)	m_G (kg/s)	System pressure (MPa)
30–05 (Air–water)	0.3	0.37–0.41	0.30
30–09 (Air–water)	0.3	0.18–0.27	0.15
11–01 (Steam–water)	0.3	0.49–0.67	1.50

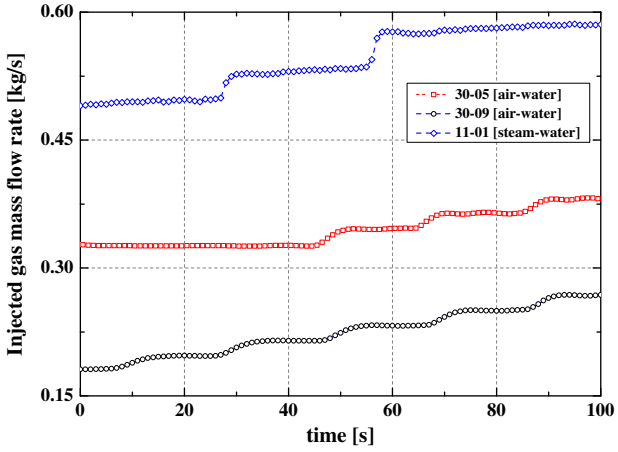

Fig. 5. Gas mass flow rate used in the calculation according to the experimental conditions.

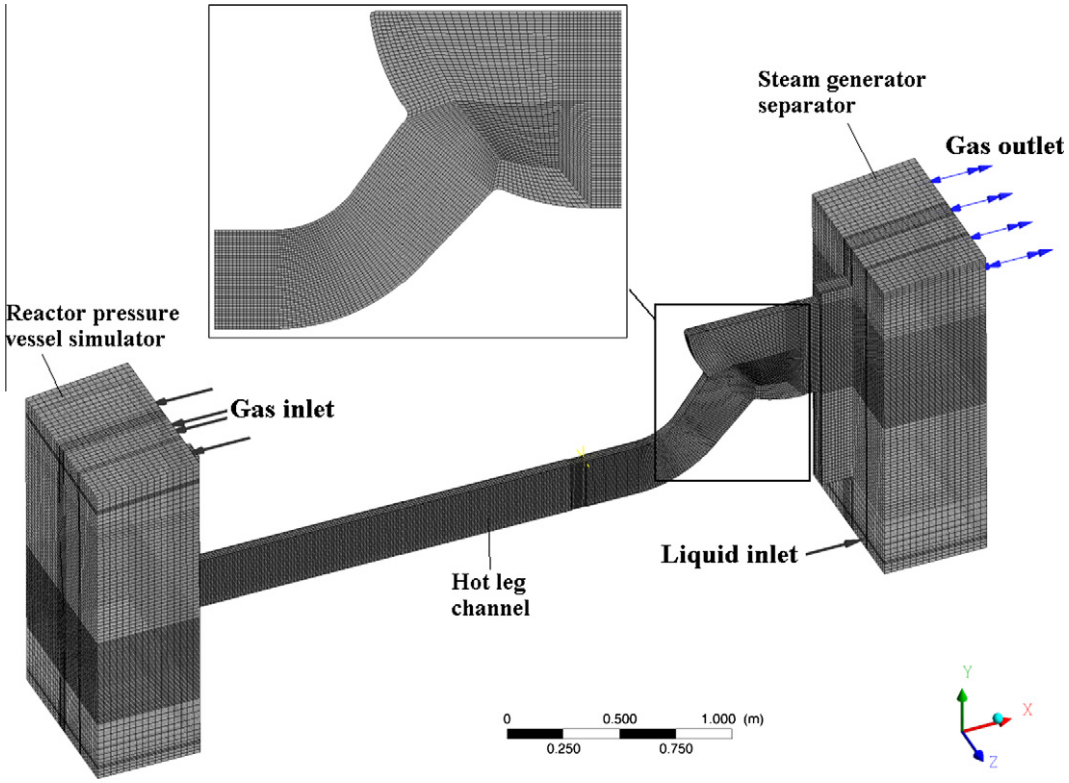

Fig. 4. Calculation model of the CCFL in PWR hot leg.

(TOPFLOW) facility at *HZDR*. Experimental data were used to check the feasibility to simulate the CCFL with existing multiphase models build in any CFD codes. The experimental apparatus and procedure used in this study were described in the previous papers (Deendarlianto et al., 2008; Vallée et al., 2009). The main components consist of the test section, the reactor pressure vessel (RPV) simulator located at the lower end of the horizontal channel and the steam generator (SG) separator located at the upper end of the inclined channel. The test section is composed of a horizontal rectangular channel, a bend that connects it to an upward inclined and expended channel, and a quarter of a circle representing the steam generator inlet chamber. The horizontal part of test section is 2.12 m long and has a rectangular cross-section of 0.05 m $\times$ 0.25 m. The riser is 0.23 m long, has an inclination of 50° to the horizontal plane and an expansion angle of 7.5°. Both the SG and RPV simulators are identical vessels with 0.8 m $\times$ 0.5 m $\times$ 1.55 m ($D \times W \times H$) cubic shape. The water levels in both separators were determined by the measurement of the differential pressure between the top and the bottom of the vessels with differential pressure transducers. Next, the differential pressure between the SG and RPV simulators was measured by a differential pressure transducer. The signals of the pressure sensors, the water levels inside both separators, injection mass flow rates and temperatures of air and water, and the air pressure inside the test vessel were transmitted to a personal computer via a data acquisition system running at 1 Hz. In addition, the experimental apparatus is put in a pressure tank, where it was operated in pressure equilibrium with the inner atmosphere of the tank as shown in Fig. 3.

In the present CFD simulations, the following boundaries were used. The inhomogeneous multiphase model was implemented. Very carefully developed structured mesh for most of the flow field was adequate, at which the local refinement on them were carried out. The effect of numerical diffusion can be minimized by using meshes with a finer resolution, higher order discretisation methods and suitable time step sizes. Here a structured mesh consisted

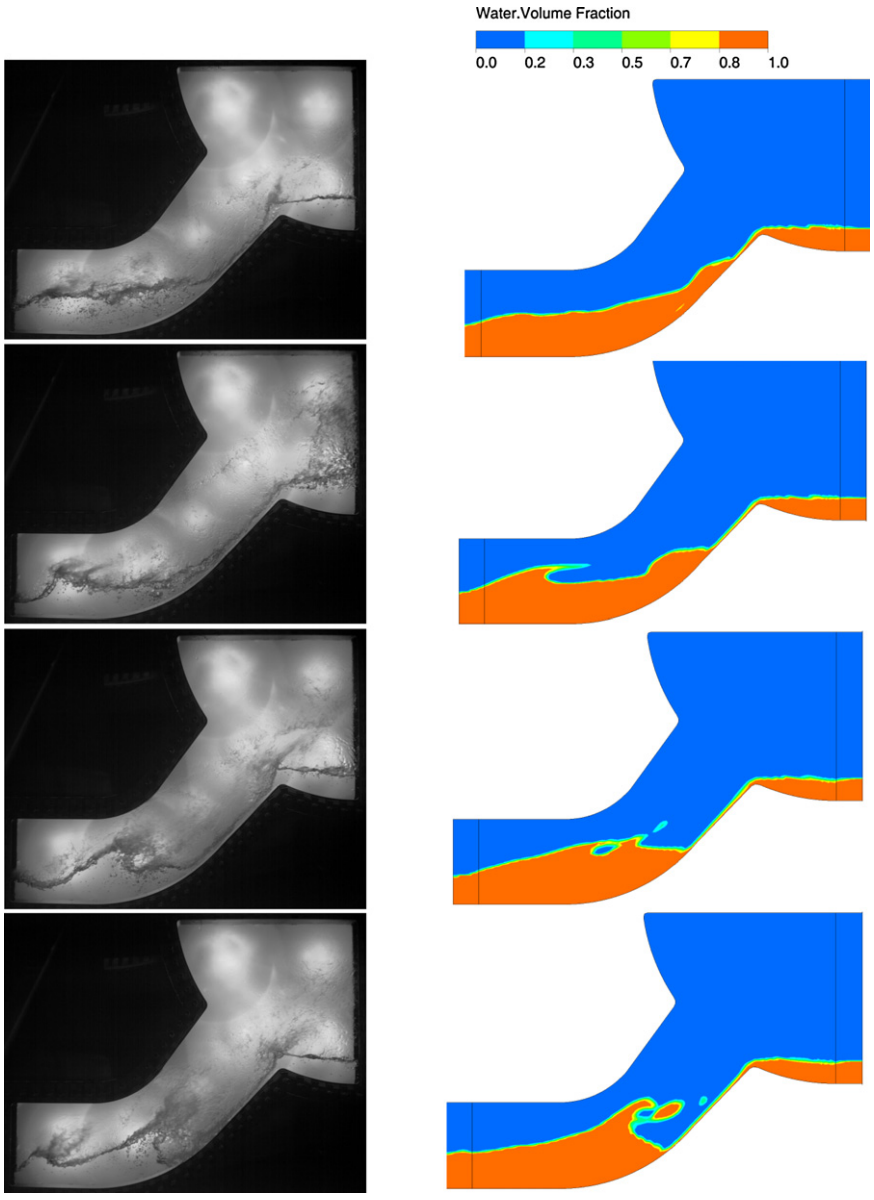

(a) Experiment (b) Calculation

Fig. 6. Time series of wave crest around the CCFL of the steam–water case (m_G = 0.533 kg/s).

of 248,610 hexahedral elements and 281,076 nodes as shown in Fig. 4.

Two air–water (*HZDR* experimental run of 30–05 and 30–09) and one steam–water (experimental run of 11–01) CCFL experiments were selected from *HZDR* test series, and they are summarized in Table 1. In the calculation, the injected gas flow rates were used in current calculation according to experimental conditions as shown in Fig. 5. The time step of the transient calculation was $\Delta t = 10^{-04}$ s. Next, the SST buoyancy turbulence model was employed. Moreover, the newly drag coefficient, C_D, in AIAD model (Eq. (13)) was implemented into ANSYS CFX via the command language CEL (CFX expression language). The calculations were performed in parallel of four processors of HZDR Linux cluster. Typical computation time for each case was about 4 months.

In order to examine the usefulness of new developed drag coefficient, a transient simulation was carried firstly by using a constant drag coefficient of $C_D = 0.44$ as a default value from ANSYS CFX. A selected case of HZDR experimental run of 30–09 was used. The results were reported in previous paper (Deendarlianto et al., in press). They mentioned that the formation of liquid slug and wave crest during CCFL as observed in experiment could not reproduced by using $C_D = 0.44$. This means that $C_D = 0.44$ is not big enough to promote a liquid slug and break during CCFL in the hot leg channel. It indicates also that the choosing of interfacial friction seems to be very important for the simulation of wave crest during flooding.

Fig. 6 shows comparatively a series of wave crest near the bend during CCFL of PWR hot leg obtained from experiment and corresponding CFD calculation, in which the new drag coefficient in AIAD model was implemented in CFD calculation. The test fluids were steam and water. The steam mass flow rate was 0.533 kg/s. The time step of corresponding pictures was 0.1 s. In both cases, a big wave is developing and breaking down by the steam flow. The calculated wave form is in good agreement with the experiment. The entrainment of small liquid droplet in front of wave obtained from experiment could be observed also by the calculations as shown clearly in Fig. 6b. This result indicates that the developed drag coefficient in AIAD model has a capability to simulate the wave formation and its break-down during CCFL of a stratified counter-current flow.

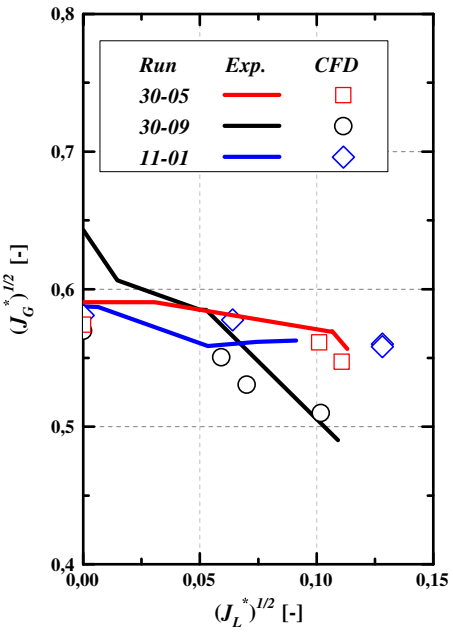

Fig. 7. CCFL characteristics.

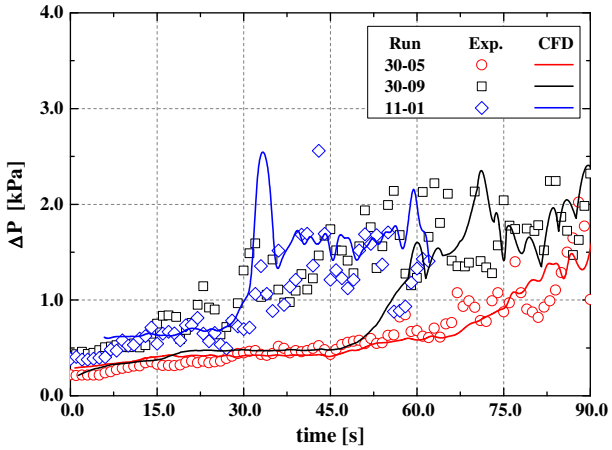

Fig. 8. Transient pressure difference between RPV and SG separators for experiments and CFD simulations.

Fig. 7 shows a comparison of the CCFL characteristics between the CFD calculation and experiment. The comparison is represented in the Wallis parameter J_k^*, and is defined as follows:

$$J_k^* = J_k \sqrt{\frac{1}{gH} \cdot \frac{\rho_k}{(\rho_L - \rho_G)}} \tag{14}$$

where the subscript k indicates gas and liquid phases, J the superficial velocity, ρ the density, g the acceleration of gravity, and H the height of the channel. Close inspection of Fig. 7 reveals that the calculated CCFL is qualitatively correct according to the HZDR experimental data.

The pressure difference between RPV and SG separators taken from experiments and CFD calculations are shown in Fig. 8. Close observation of this reveals that the transient pressure difference between both simulators can be simulated. In general, the calculated pressure difference is in agreement with the experimental data. Furthermore a small deviation of the peak pressure difference is observed (experimental run of 11-01 at $t = 34$ s as an example). This is due to the measurement frequency is much lower than the calculated values; therefore some peak pressure difference was detected from the experiment.

In order to capture the water level data along hot leg channel obtained from experiment, an image processing technique was developed. The data was compared with CFD calculation as shown

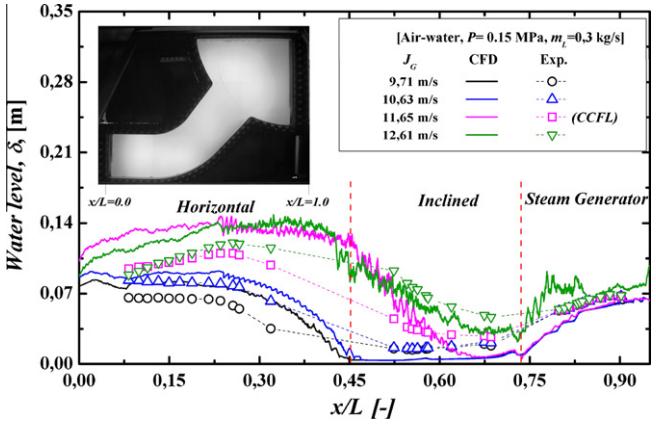

Fig. 9. Water level inside the hot leg channel (experimental run of 30–09).

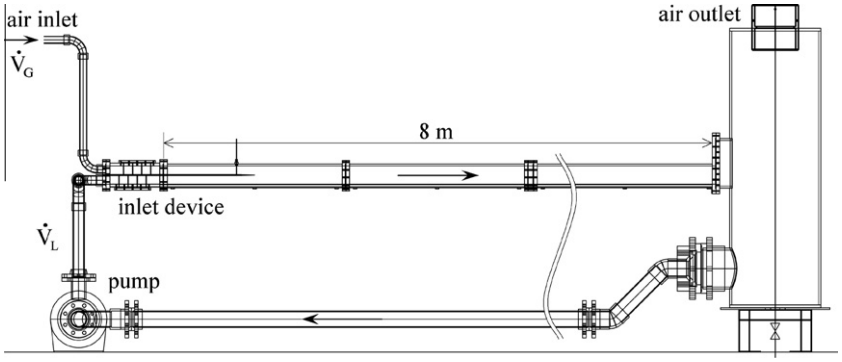

Fig. 10. Schematic view of the horizontal channel HAWAC with inlet device for a separate injection of water and air into the test-section.

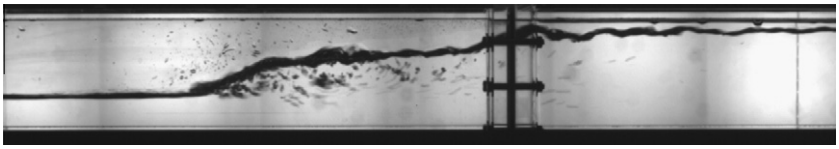

Fig. 11. Example of the observed hydraulic jump at HAWAC.

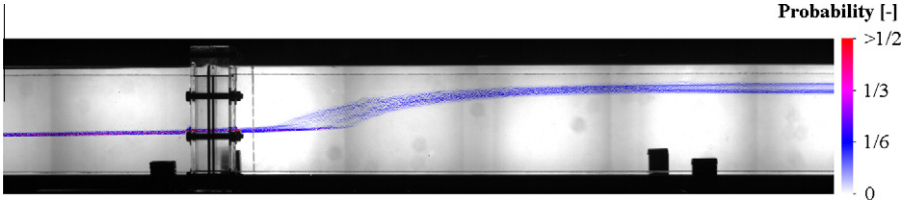

Fig. 12. Representation of the probability distribution of the water level measured in a hydraulic jump.

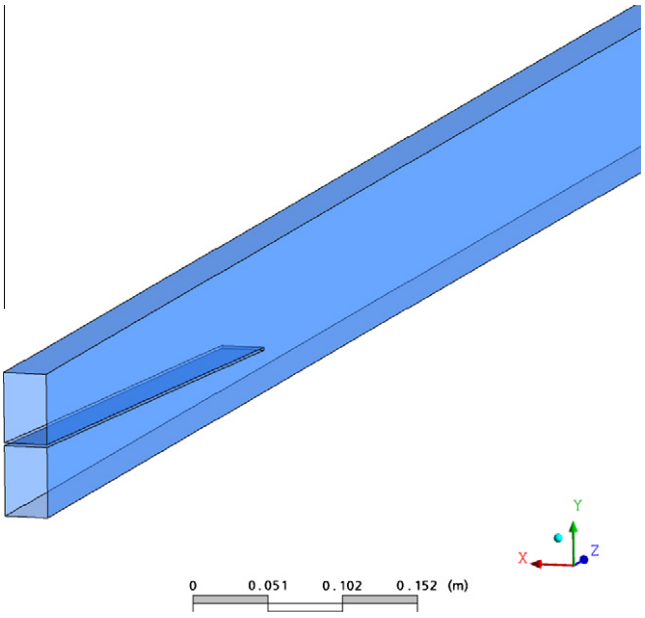

Fig. 13. Grid model with blade in declined position (zoom inlet part).

Table 2
Comparison of water levels between measurement and calculation.

	Experiment	CFD calculation
Water level h_2 (mm)	90 ± 3	90
Water level h_1 (mm)	36.75 ± 1.5	32.3 ± 3.1

in Fig. 9. This figure reveals that the calculated time average water levels and their trends are in agreement with the experimental data. Furthermore a small deviation is observed when the gas velocity approaches the CCFL. This occurs due to the difficulty in the detection of the water level in the pictures obtained from experiment caused of the occurrence of mixed flow layer near the interface.

4.2. Hydraulic jump during the air/water co-current two-phase in a horizontal channel

The hydraulic jump flow regime is an effective scenario for free surface model validation, as the hydraulic jump mostly occurs at steady state conditions with high turbulence at the free surface and inclined water levels. The hydraulic jump is the discontinuous transition between super- and sub-critical flow, and is well-known in open channel flow (Henderson, 1966). It is characterized by a steep rising of the water surface with a high turbulence zone and possible gas entrainment. Despite occurrence in tunnel spillways, drainage and sewer engineering, the hydraulic jump has received poor attention in closed conduits (Stahl and Hager, 1999).

For the experimental investigation of air–water flows, HAWAC (Horizontal Air–Water Channel) with rectangular cross-section (Fig. 10) was built at HZDR. Its inlet device provides defined inlet boundary conditions. The channel allows in particular the study of hydraulic jumps and air/water slug flow regimes under atmospheric pressure. Parallel to the experiments, CFD calculations were carried out (Höhne and Vallée, 2010). Other groups (Bartosiewicz et al. (2010)) also used the experiments at the HAWAC channel as a benchmark study for stratified two-phase flows

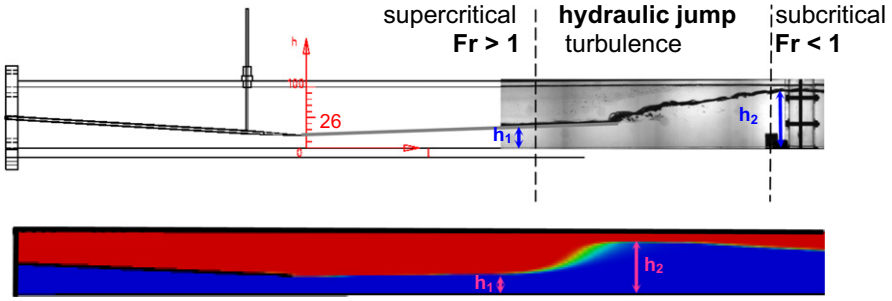

Fig. 14. The comparison on the hydraulic jump profile between experiment (upper figure) and CFD calculation (lower figure) that indicates the zones of air/water co-current stratified flow in a horizontal channel (supercritical zone, hydraulic jump, subcritical zone).

in the frame of the European Platform for NUclear REactor SIMulations (NURESIM).

The experimental apparatus, procedure and experimental result were described in Vallée et al. (2008), an main feature will be presented here. A special inlet device provides defined inlet boundary conditions by a separate injection of water and air into the test-section. The cross-section of the channel are $100 \times 30\ mm^2$ (height $\times$ width). The test-section is about 8 m long. Four wire mesh filters made of stainless steel wires (diameter of 0.63 mm and mesh size of 1.06 mm) are mounted to provide a homogeneous velocity profiles at the test-section inlet. The free inlet cross-section for each phase can be controlled by inclining this blade up and down. At the HAWAC test facility at high water flow rates, especially when the inlet blade is inclined down, a hydraulic jump can be realized in the test-section (Fig. 11). High-speed video observation was applied and an algorithm was developed to recognize the interface in the camera frames. From this data, the water level can be extracted in any cross-section. Since the interface is very dynamic due to the high turbulence in the hydraulic jump, a statistical approach is proposed in order to reflect the structure of the interface over the time. The probability distribution of the water levels was calculated in each vertical cross-section and is shown according to a colored scale in Fig. 12. Experiments were performed to point out the influence of the air flow rate on the hydraulic jump in a closed channel. Therefore, the water flow rate and the inlet blade position were kept constant. Observations show that the position of the hydraulic jump from the inlet is very sensitive to the air superficial velocity in the test-section (Fig. 10). This is due to the momentum exchange between the phases. Furthermore, the growing distance between minimum and maximum jump positions reflects the increasing smearing of the probability distribution with higher air flow rate. These experimental data can be useful to validate the modeling of the momentum exchange in CFD-codes applied to stratified two-phase flow regimes.

The aim of the numerical simulations presented in this chapter is the validation of prediction a hydraulic jump with newly developed and implemented multiphase flow models. The CFD calculation was performed using a grid of 930,000 nodes (hexahedral elements). The blade was modeled in 2.75° downward position (Fig. 13). At the inlet water was modeled in the lower 50% of the inlet cross section (under the blade) and air in the upper 50% (above the blade). The time step of the transient calculation was $\Delta t = 10^{-05}$ s. The k–ϖ turbulence model and the turbulence damping functions were used. The boundary conditions correspond to the *HZDR* measurement run of 03. The superficial velocities of water and air were 0.467 m/s and 0.103 m/s, respectively. The water and air temperatures were 22 °C.

As shown in Fig. 14, the hydraulic jump could be simulated successfully. Quantitatively it agrees well with the experimental observation. Next it is noticed that the experiment and the CFD calculation show the similar characteristics: the supercritical region, the area of the hydraulic jump and the subcritical region. The local character of the liquid flow is described in a cross-section by the Froude number:

$$\mathrm{Fr} = \frac{\dot{V}}{W \cdot h} \cdot \frac{1}{\sqrt{g \cdot h}} \tag{15}$$

where $\dot{V}$ is the liquid volume flow rate, W the channel width, g the acceleration of gravity and h the water level in the cross-section.

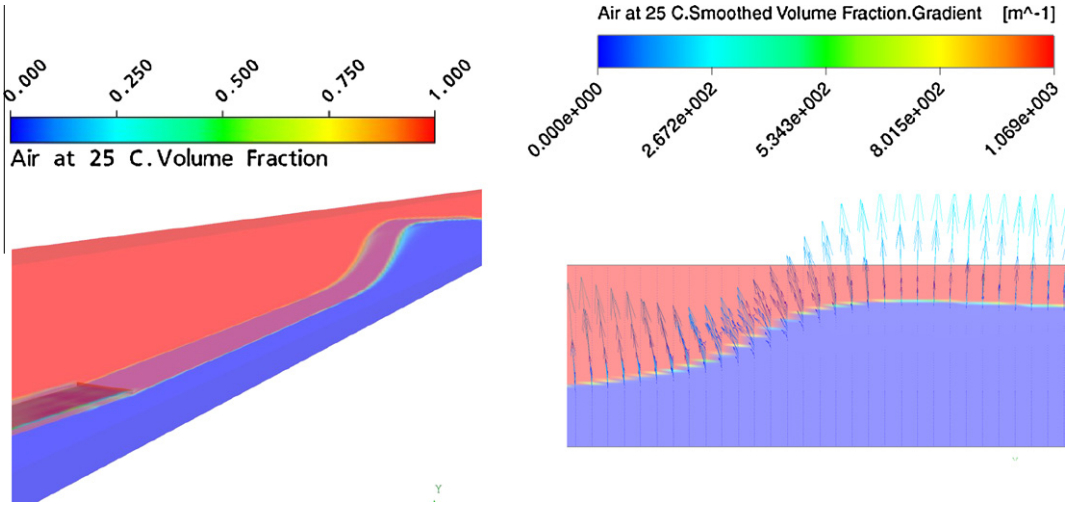

Fig. 15. The calculated air-volume fraction (left) and its gradient (right).

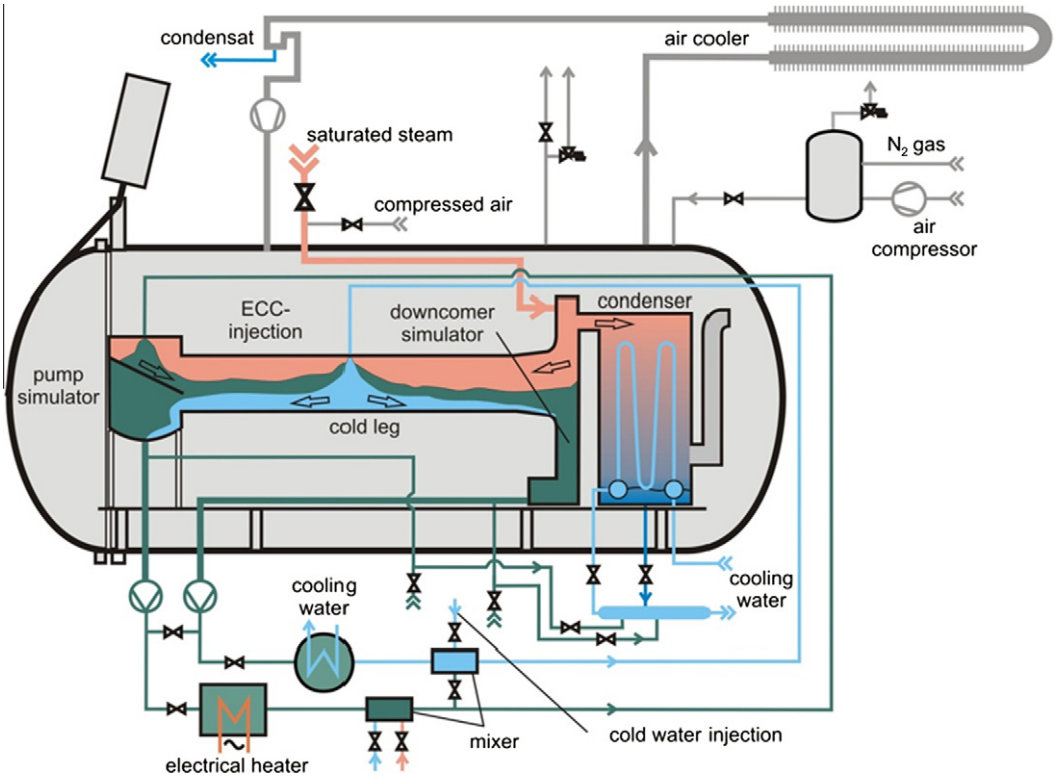

Fig. 16. Schematic diagram of PTS experimental at TOPFLOW facility.

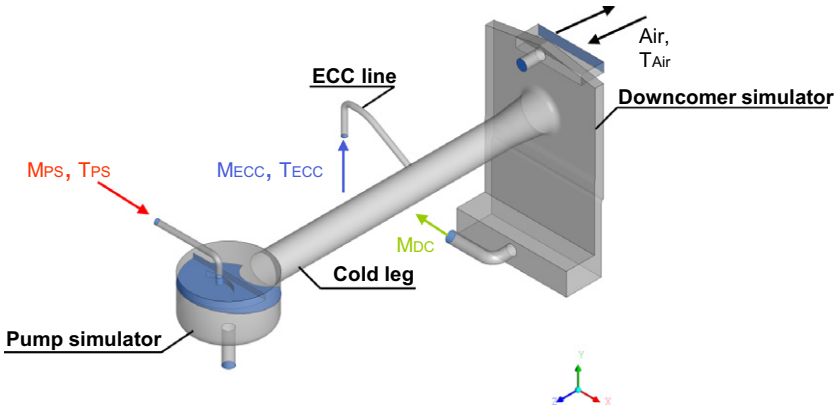

Fig. 17. Boundary conditions for the air–water test.

The flow is supercritical when the local Froude number (Fr_L) is larger than unity and else subcritical. Moreover, the calculated heights h_1 and h_2 were in agreement also with the experimental data as shown in Table 2. In addition it is found that the calculated of water level rising is steeper than that of experiment, whereas the length of the hydraulic jump has been underestimated in the calculation.

In the free surface calculation without AIAD model, the rise of the water level in hydraulic jump is smeared (the result is not shown here). Meanwhile it was improved by using the AIAD model as shown in Fig. 15. In the figure, the left and right sides show the air volume fraction and the gradient of the air volume fraction, respectively. This gradient is used for calculating the momentum exchange at the free surface according to Eq. (13).

4.3. Pressurized thermal shock (PTS)

Pressurized thermal shock (PTS) has been identified as one of the most important industrial needs related to nuclear reactor safety. It occurs when there are large thermal loads on the re-actor pressure vessel (RPV) wall. The PTS analysis is required to ensure the integrity of the RPV throughout the reactor life. Several scenarios that describe the phenomena in *Small Break Loss Of Coolant Accidents* (SB-LOCA) result in an emergency core cooling (ECC) water injection into the cold leg of a PWR. The cold water in the cold leg mixes with the hot coolant, which is present in the primary circuit. The mixture flows to the downcomer where further mixing of the fluids takes place. During the two-phase PTS situations the water level in the RPV has dropped down to or below the height of the cold leg nozzle, which leads to a partially filled or totally uncovered cold leg. In order to predict thermal gradients in the structural components of RPV wall, knowledge of transient temperature distribution in the downcomer is needed. For the prediction of the temperature distribution, reliable CFD simulations are required. The CFD models should be able to model the complex mixing processes taking place in the cold leg and the downcomer of the RPV (IAEA, 2001; Lucas et al., 2009a,b). Currently available

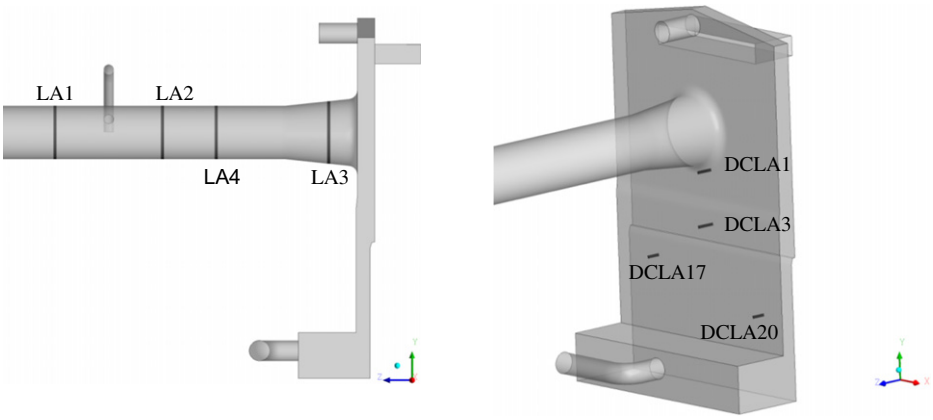

Fig. 18. Locations of the thermocouples lances in the cold leg (left) and the downcomer (right).

CFD codes are not able to simulate accurately all phenomena that occur in the cold leg and the downcomer during the ECC injection. Numerical simulations have already been performed with moderate success; see, e.g. the contributions of Egorov (2004), Vallée et al. (2005), Štrubelj and Tiselj (2007), Coste et al. (2008, 2010) and Tiselj et al. (2006).

In the framework of the EU NURISP project (Nuclear Reactor Integrated Simulation Project) attempts are being made to improve the CFD modeling for the two-phase PTS situations. For this purpose, two reference cases from the TOPFLOW-PTS experimental programme were defined: one for steady air–water and one for steady steam–water flow (Peturaud et al., submitted for publication). In the current paper numerical simulations of the air–water experiment will be presented.

The air–water PTS experiment was carried out at the TOPFLOW-PTS test facility of the HZDR (Fig. 15). The EDF CPY 900 MWe PWR was defined as the reference plant for the test facility with a geometrical scale of 1:2.5. The test facility was designed in a way to simplify the configuration in order to allow better access for instrumentation and analysis of the results. It is composed of a flat

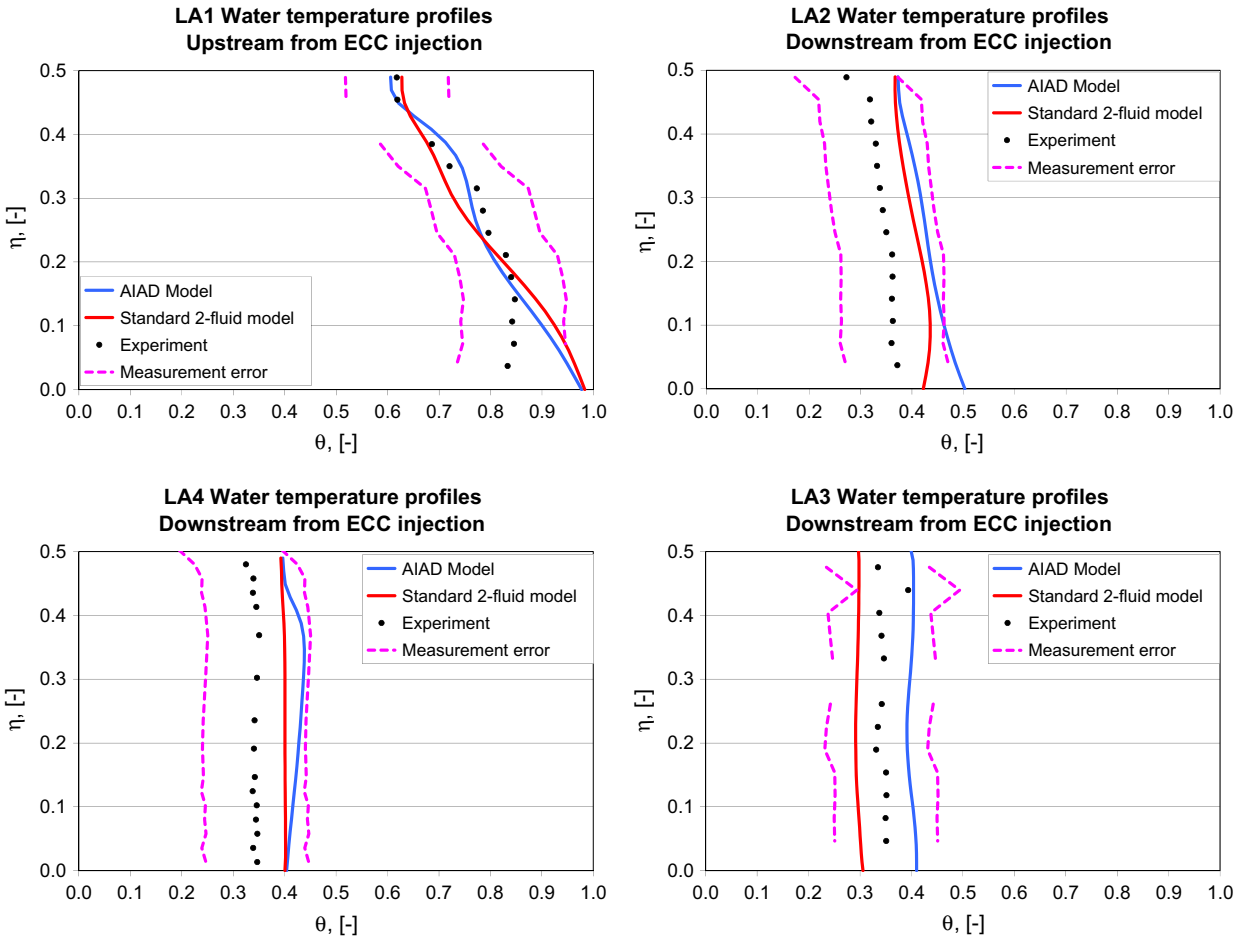

Fig. 19. Temperature profiles in the cold leg.

downcomer and a pump simulator, which is connected by a cold leg (cf. Fig. 16). In the selected steady state air–water experiment, the cold leg was 50% full of water. The operating pressure was P_0 (2.25 MPa). The cold ECC water was injected into the cold leg through the ECC line. The hot water was injected into the pump simulator from the top and flowed to the downcomer. All of the injected water flow was withdrawn from the bottom of the downcomer.

According to the design of the test facility, the pump simulator, the cold leg with the ECC line and the flat downcomer were included to the CFD Model (Fig. 17). The geometrical model was generated using the CAD software Autodesk Inventor 2009. ICEM CFD software was used to generate the numerical grid. The grid consists of approximately 1450,000 hexagonal elements. For the generation of the geometry and the grid best practice guidelines were considered as far as was possible.

In the simulation, the boundary conditions were defined as follows (see Fig. 17). The cold leg was 50% full of water. The mass flow rate of ECC injection was MECC and the temperature of ECC water was TECC. The mass flow rate and temperature of pump simulator injection were MPS and TPS respectively. The ratio of the mass flow rate of pump simulator to the mass flow rate of ECC injection was 1:1.7. The outlet water mass flow rate MDC was calculated as MPS + MECC. The fluid properties varied with pressure and temperature. The water table from the International Association for the Properties of Water and Steam (IAPWS) was applied for water. The air was considered as a perfect ideal gas.

The simulations were performed using the standard two-fluid model available in the ANSYS CFX and the AIAD model. Turbulence was modeled with SST model. In the present study, the simulations were performed according to the best practice guidelines (BPGs) described by Menter (2002). They were performed at HZDR LINUX cluster (Operating system: Linux Scientific 4.3 (64 bit), Node configuration: 2xAMD Opteron F 2220 (2.8 GHz, dual-core), 16 GB Memory). Four nodes (16 processors) were used for the transient simulation. The simulations took two months each to complete.

A steady state was reached when RMS normalized values of the equation residuals became lower than 1×10^{-5} and the fluctuations of main physical variables (temperature, velocity, etc.) at different locations in the cold leg and the downcomer were negligible. Eight locations were selected in the cold leg and the downcomer, which show the local temperature distribution (cf. Fig. 18). The locations correspond to the positions of the thermocouples used in the cold leg and the downcomer. In the cold leg, the thermocouple lance LA1 is located upstream from the ECC injection point and the thermocouple lances LA2, LA4 and LA3 are located downstream from the ECC injection point. Thermocouples DCLA1, DCLA3, DCLA17 and DCLA20 are located in the downcomer.

To present the results in a dimensionless form, non-dimensional coordinates η, ζ and temperature θ were defined as follows

$$\eta = 0 \div 1 \tag{16}$$

$$\zeta = y/D_{CL} \tag{17}$$

$$\theta = \frac{T - T_{ECC}}{T_{PS} - T_{ECC}} \tag{18}$$

where $\eta = 0$ corresponds to empty cold leg, while $\eta = 1$ corresponds to a fully filled cold leg. D_{CL} is the inner diameter of the cold leg. Fig. 19 shows the comparison of the dimensionless form of the temperature profiles in the cold leg between the calculations and the

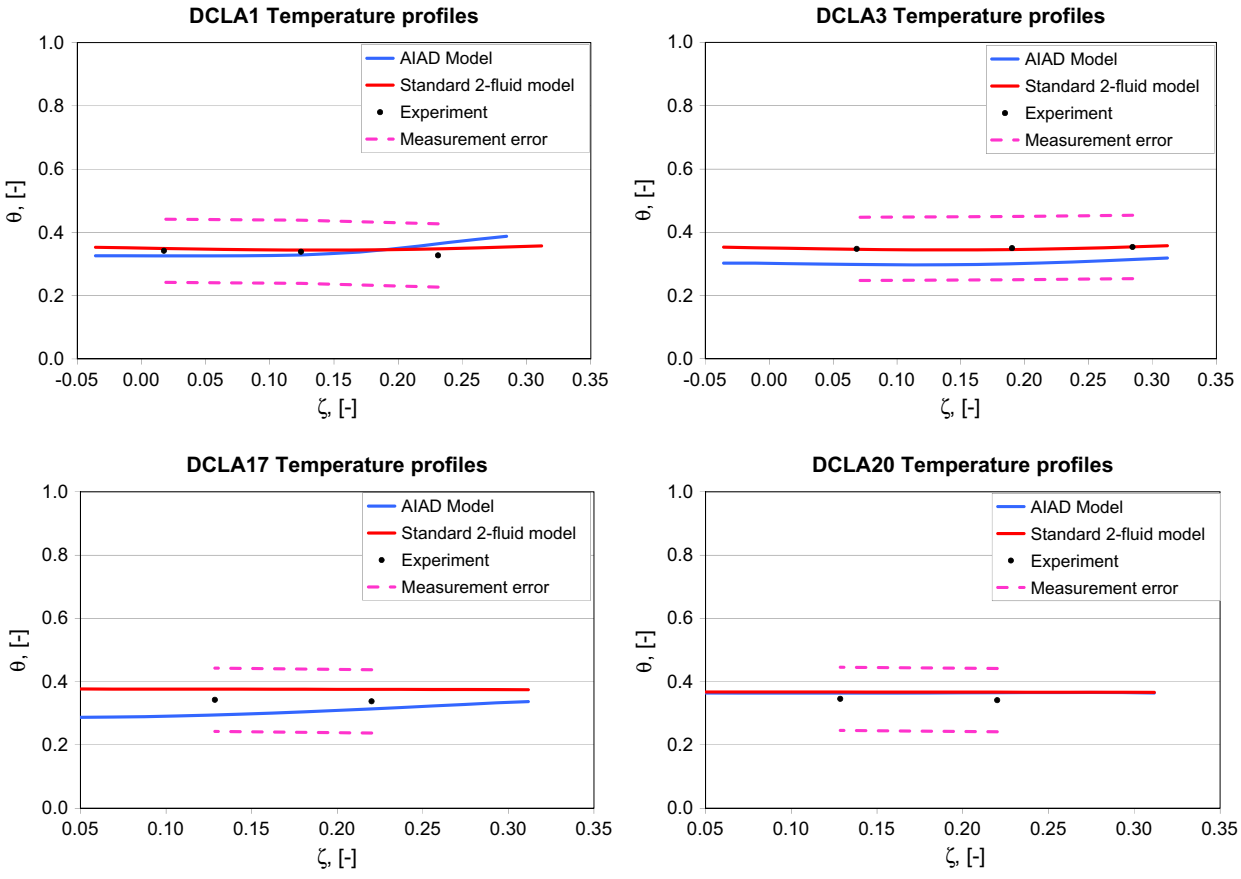

Fig. 20. Temperature profiles in the downcomer.

experiment. Experimental data shows that there is only a temperature gradient in the water in the region upstream of the cold leg ECC injection. Downstream of ECC, the liquids are well mixed and the water temperature is approximately equal to perfect mixed temperature. It is noticeable that both models provide fairly similar results. A comparison between the CFD simulations and the experiment shows that the calculated temperature profiles are in good agreement with those from experiment. The deviations are in the range of the measurement accuracy. It amounts to approximately ±1 K.

Fig. 20 shows calculated and measured temperature profiles at the selected locations in the downcomer. The position of the reverse wall in the upper part of the downcomer belongs to $\zeta = -0.035$. In the lower part, the corresponding value is $\zeta = 0.05$.

Generally the calculated temperature profiles are in agreement with those of experiment. The water temperature at all four locations is homogeneous and it is equal to the perfect mixed temperature, i.e. there is no thermal stratification in the downcomer.

5. Conclusions and outlooks

The new concept of the drag coefficient in the AIAD model was implemented into a CFD code for a better description of the 3-D phenomena relate to nuclear reactor safety analysis. Those include the prediction of counter-current flow limitations (CCFL) in a PWR hot leg, the development of hydraulic jump during the air/water co-current flow in a horizontal channel, and pressurized thermal shock (PTS) phenomena in a PWR cold leg and downcomer. The presented results showed a clear progress in the simulation of the relevant phenomena.

Nevertheless, further improvement and validation of the model should be carried out. The effect of mass transfer should be included in the future. Next, turbulence damping procedures at the free surface should consider the existence of small surface instabilities in the macroscopic model. The numerical approach of the AIAD model should be improved to further reduce the calculation time. Modeling of non-drag forces (lift force, wall lubrication force, virtual mass force, etc.) in the AIAD model should be also considered. The final goal is to provide an easy usable AIAD framework for all code users.

Acknowledgements

The experimental and theoretical works on the CCFL in a PWR hot leg and hydraulic jump in a horizontal channel are carried out within the frame work of a current research project funded by the German Federal Ministry of Economics and Technology, project number 150 1329 (TOPFLOW 2 project).

Theoretical investigations of pressurized thermal shock are financially supported by the NURISP (NUclear Reactor Integrated Simulation Project) project. The NURISP project is partly funded by the European Commission in the framework of the Seventh Framework Program EURATOM (2009–2011). The TOPFLOW-PTS Experiments Project is financially supported by CEA, EDF, IRSN, AREVA (France); PSI, ETHZ (Switzerland) and HZDR (Germany).

The authors would like to thank also the TOPFLOW team for their work on the test facility and the experiments. We would like to thanks also Yuri Egorov and Thomas Frank from ANSYS Germany for their fruitful cooperation.

Dr. Deendarlianto is an *Alexander von Humboldt* Fellow in the Institute of Safety Research, *Helmholtz-Zentrum Dresden-Rossendorf e.V.*, Dresden, Germany. A part of the present research (CCFL in a PWR hot leg) is also supported by the *Alexander von Humboldt Foundation* in Germany.

References

Bartosiewicz, Y., Seynhaeve, J.-M., Vallee, C., Höhne, T., Laviéville, J., 2010. Modeling free surface flows relevant to a PTS scenario: comparison between experimental data and three RANS based CFD-codes – comments on the CFD-experiment integration and best practice guideline. Nuclear Engineering and Design 240, 2375–2381.

Ĉerne, G., Petelin, S., Tiselj, I., 2001. Coupling of the interface tracking and the two-fluid models for the simulation of incompressible two-phase flow. Journal of Computational Physics 171 (2), 776–804.

Coste, P., Laviéville, J., Pouvreau, J., Boucker, M., 2008. A two-phase CFD approach to the PTS problem evaluated on COSI experiment. In: Proceedings of the 16th International Conference on Nuclear Engineering ICONE16, May 11–15. Orlando, Florida, USA.

Coste, P., Laviéville, J., Pouvreau, J., Baudry, C., Guingo, M., Douce, A., 2010. Validation of the large interface method of NEPTUNE_CFD 1.0.8 for pressurized thermal shock (PTS) applications. In: Proceedings of CFD4NRS, 14–16 September. Washington, DC, USA.

Deendarlianto, Vallée C., Lucas, D., Beyer, M., Pietruske, H., Carl, H., 2008. Experimental study on the air/water counter-current flow limitation in a model of the hot leg of a pressurized water reactor. Nuclear Engineering and Design 238 (12), 3389–3402.

Deendarlianto, Höhne T., Lucas, D., Vierow, K., submitted for publication. Gas–liquid countercurrent two-phase flow in a PWR hot leg: a comprehensive research review. Nuclear Engineering and Design.

Deendarlianto, Höhne T., Lucas, D., Montoya, G.A., Vallée, C., in press. CFD simulation of counter-current two-phase flow in a model of the hot leg of pressurized water reactor (PWR). In: 19th International Conference on Nuclear Engineering (ICONE 19), May 16–19. Chiba, Japan.

Egorov, Y., 2004. Validation of CFD codes with PTS-relevant test cases. In: 5th Euratom Framework Programme ECORA project.

Harlow, F.H., Welch, J.E., 1965. Numerical calculation of time-dependent viscous incompressible flow of fluid with free surface. Physics of Fluids 8 (12), 2182–2189.

Hirt, C.W., Nichols, B.D., 1981. Volume of fluid (VOF) method for the dynamics of free boundaries. Journal of Computational Physics 39 (1), 201–225.

Höhne, T., 2009. Experiments and numerical simulations of horizontal two-phase flow regimes. In: Proceeding of the Seventh International Conference on CFD in the Minerals and Process Industries. Melbourne, Australia.

Höhne, T., Vallée, C., 2010. Experimental and numerical simulations of horizontal two-phase flow regimes using an interfacial area density model. The Journal of Computational Multiphase Flow 2 (3), 131–143.

IAEA, 2001. Guidelines on pressurized thermal shock analysis for WWER nuclear power plants. IAEA Document IAEA-EBP-WWER-08.

Lucas, D., Bestion, D., Bodèle, E., Coste, P., Scheuerer, M., D'Auria, F., Mazzini, D., Smith, B., Tiselj, I., Martin, A., Lakehal, D., Seynhaeve, J.-M., Kyrki-Rajamäki, R., Ilvonen, M., Macek, J., 2009a. An overview of the pressurized thermal shock issue in the context of the NURESIM project. Science and Technology of Nuclear Installations 2009, 583259.

Lucas, D., Bestion, D., Coste, P., Pouvreau, J., Morel, Ch., Martin, A., Boucker, M., Bodele, E., Schmidtke, M., Scheuerer, M., Smith, B., Dhotre, M.T., Niceno, B., Lakehal, D., Galassi, M.C., Mazzini, D., D'Auria, F., Bartosiewicz, Y., Seynhaeve, J.-M., Tiselj, I., ŠTrubelj, L., Ilvonen, M., Kyrki-Rajamäki, R., Tanskanen, V., Laine, M., Puustinen, J., 2009b. Main results of the European project NURESIM on the CFD-modelling of two-phase pressurized thermal shock (PTS). Kerntechnik 74, 238–242.

Menter, F., 2002. CFD best practice guidelines for CFD code validation for reactor safety applications. ECORA FIKS-CT-2001-00154.

Minami, N., Utanohara, Y., Kinoshita, I., Murase, M., Tomiyama, A., 2009. Numerical calculations on countercurrent gas–liquid flow in a PWR hot leg (1) air–water flow in a 1/15-scale model. In: Proceeding of the 13th International Topical Meeting on Nuclear Reactor Thermal Hydraulics (NURETH-13), September 2009. Kanazawa City, Japan.

Murase, M., Utanohara, Y., Kinoshita, I., Minami, N., Tomiyama, A., 2009. Numerical calculations on countercurrent air–water flow in small-scale models of a PWR hot leg using a VOF model. In: Proceeding of the 17th International Conference on Nuclear Engineering (ICONE 17), July 2009. Brussels, Belgium.

Osher, S., Sethian, J.A., 1988. Front propagating with curvature dependent speed: algorithm based on Hamilton–Jacob formulations. Journal of Computational Physics 79, 12–49.

Peturaud, P., Hampel, U., Barbier, A., Dreier, J., Dubois, F., Hervieu, E., Martin, A., Prasser, H.-M., submitted for publication. General overview of the TOPFLOW-PTS experimental program. In: 14th International Topical Meeting on Nuclear reactor Thermal Hydraulics (NURETH-14), September 25–29, 2011. Toronto, Ontario, Canada.

Stahl, H., Hager, W.H., 1999. Hydraulic jump in circular pipes. Canadian Journal of Civil Engineering 26, 368–373.

Štrubelj, L., Tiselj, I., 2007. Numerical modelling of condensation of saturated steam on sub-cooled water surface in horizontally stratified flow. In: Proceedings of the 12th International Topical Meeting on Nuclear Reactor Thermal Hydraulics (NURETH-12), Sheraton Station Square, September 30–October 4. Pittsburgh, Pennsylvania, USA.

Štrubelj, L., Tiselj, I., Mavko, B., 2009. Simulations of free surface flows with implementation of surface tension and interface sharpening in the two-fluid model. International Journal of Heat and Fluid Flow 30 (4), 741–750.

Tiselj, I., Štrubelj, L., Prošek, A., 2006. Direct contact condensation in horizontally stratified flow of AEKI PMK-2 device. In: 6th Euratom Framework Program NURESIM, Deliverable D2.1.13.1.

Vallée, C., Höhne, T., Prasser, H.-M., Sühnel, T., 2005. Experimental investigation and CFD simulation of air/water flow in a horizontal channel. In: Processing of the 11th International Topical Meeting on Nuclear Reactor Thermal-Hydraulics (NURETH-11). Avignon, France.

Vallée, C., Höhne, T., Prasser, H.-M., Sühnel, T., 2008. Experimental investigation and CFD simulation of horizontal stratified two-phase flow phenomena. Nuclear Engineering and Design 238 (3), 637–646.

Vallée, C., Seidel, T., Lucas, D., Beyer, M., Prasser, H.-M., Pietruske, H., Schütz, P., Carl, H., 2009. Influence of the fluid properties on co-current two-phase flows in a horizontal channel connected to a riser. In: Proceedings of the 7th World Conference on Experimental Heat Transfer, Fluid Mechanics and Thermodynamics (ExHFT-7), 28.06.–03.07.2009. Krakow, Poland, pp. 443–452.

Wang, M.J., Mayinger, F., 1995. Simulation and analysis of thermal-hydraulic phenomena in a PWR hot leg related to SBLOCA. Nuclear Engineering and Design 155, 643–652.